Micromagnetic Simulation of the Pinning and Depinning Process in Permanent Magnets

Werner Scholz, Thomas Schrefl, Josef Fidler, Thorsten Matthias, Dieter Suess, and Vassilios Tsiantos

Abstract—We have studied the pinning of magnetic domain walls on a simplified model of the cell structure of $Sm(Co,Fe,Cu,Zr)_z$ precipitation hardened magnets. The pinning field strongly depends on the thickness of the intercellular phase if it is smaller than the domain wall width. Its maximum value has been verified with a one-dimensional analytical model. The cell structure plays an important role in the depinning process and it has been found that the pinning field depends linearly on the relative thickness of the intercellular phase. This behavior is universal for attractive and repulsive pinning.

Index Terms—Domain wall pinning, finite-element method, micromagnetics, SmCo.

TABLE I
MATERIAL PARAMETERS OF TYPICAL $Sm(Co,Fe,Cu,Zr)_z$ PERMANENT MAGNETS [7]–[9]

	"2:17" type cells	"1:5" type boundary phase
J_s (T)	1.3	0.8
A (pJ/m)	14.0	14.0
K_1 (MJ/m^3)	5.0	9.0
$l_{ex} = \sqrt{A/K_1}$ (nm)	1.7	1.3
$\delta = l_{ex} \cdot \pi$ (nm)	5.3	3.9
$H_{ani} = 2K_1/J_s$ (kA/m)	7692	22500

I. INTRODUCTION

RARE EARTH permanent magnets provide the best properties for many applications. As compared with NdFeB type magnets SmCo magnets have superior properties at elevated temperatures due to their high Curie temperatures ($T_C > 1000$ K) and low-temperature coefficients of coercivity. The coercivity mechanism in $Sm(Co,Fe,Cu,Zr)_z$ magnets is based on the pinning of magnetic domain walls at the cellular precipitation structure [1]. This microstructure develops during a sophisticated and lengthy heat treatment, which includes sintering, homogenizing, quenching, isothermal aging, and annealing.

The $Sm_2(Co,Fe)_{17}$ cells are surrounded by a coherent precipitation of $Sm(Co,Fe)_5$ cell walls. The quality of this intercellular phase strongly depends on the additives, especially Zr and Cu. Cu is concentrated in the intercellular "1 : 5" phase, whereas Zr is mainly found in the lamellar structure of the Z-phase. Lorentz electron microscopy [2], [3] indicates, that the intercellular 1 : 5 phase acts as a pinning site for the magnetic domain walls, whereas the Zr rich Z-phase provides a diffusion path for Cu segregation, which results in the uniform precipitation structure. We have studied the details of this pinning mechanism using three-dimensional finite-element micromagnetic simulations.

II. FINITE ELEMENT MODEL

Our finite-element model is based on the Gibbs' free energy

$$E_{tot} = \int_V \left(\frac{A}{J_s^2} \left(\nabla \vec{J} \right)^2 - \frac{K_1}{J_s^2} \left(\vec{J} \cdot \vec{u} \right)^2 \right.$$
$$\left. - \frac{1}{2} \vec{J} \cdot \vec{H}_{demag} - \vec{J} \cdot \vec{H}_{ext} \right) dv \quad (1)$$

which includes exchange, magnetocrystalline anisotropy, demagnetization, and Zeeman energy. We use a static energy minimization method [4] to calculate the equilibrium magnetization distribution. By slowly sweeping the external field we calculate the demagnetization curve. The demagnetization field is calculated with a hybrid finite-element/boundary-element method [5].

III. PINNING ON A PLANAR INTERFACE

Our simplest geometrical model of the pinning process includes two different materials (different saturation polarization J_s, uniaxial magnetocrystalline anisotropy K_1 and exchange constant A) with a perfectly planar interface assuming a step like change [6] of the material parameters. Typical values for $Sm(Co,Fe,Cu,Zr)_z$ magnets can be found in Table I. However, the simulations depend only on the exchange length $\sqrt{A/K_1}$. If an ideal Bloch wall is assumed, the pinning field, which is required to force the domain wall into the hard material (with higher domain wall energy), can be calculated with the one-dimensional (1-D) analytical model of Kronmüller and Goll [6]. The comparison with the micromagnetic simulations shows, that the maximum edge length of the finite elements has to be smaller than the exchange length ($\sqrt{A/K_1}$, e.g., 1.7 nm in Sm_2Co_{17} [6]) of the harder material in order to avoid "artificial pinning" on the finite-element mesh. Fig. 1 shows the dependence of the pinning field H_{pin} (in units of the anisotropy field $H_{ani} = 2K_1/J_s$ of the harder material) on the ratio of exchange ($\varepsilon_A = A_{soft}/A_{hard}$) and anisotropy constants ($\varepsilon_K = K_{1,soft}/K_{1,hard}$). For $\varepsilon_A \cdot \varepsilon_K = 1$, where the two materials have equal domain wall energy, the effect of domain wall pinning and, therefore, the coercivity vanish ($H_{pin} = 0$). The pinning field is always smaller than the anisotropy field. For given ε_A (dashed line in Fig. 1) the pinning field is proportional to ε_K. However, if ε_A is reduced(which decouples the two materials) for given ε_K (solid line), the coercive field shows a steep in-
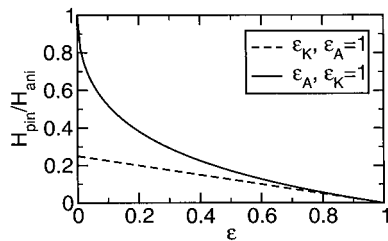
Fig. 1. Dependence of the pinning field H_{pin} (in units of the anisotropy field of the harder material) on the ratio of exchange (ε_A) and anisotropy constants (ε_K) according to a 1-D analytical model [6]. $\varepsilon_J = 1$ has been assumed for the simplicity of this graph.

Fig. 3. Pinning field for attractive and repulsive pinning as a function of the thickness t of the intercellular phase. The thickness is given in units of the exchange length of the intercellular phase. The pinning field is given in units of the pinning field for infinite t.
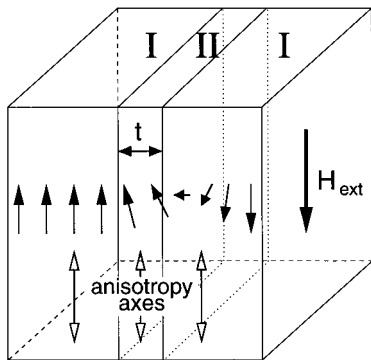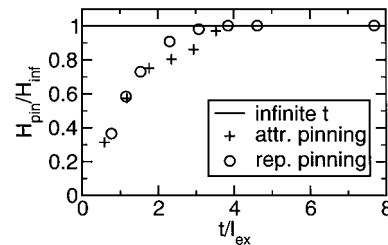

Fig. 2. Model geometry for domain wall pinning on an intercellular phase with parallel anisotropy axes. The chain of arrows indicates the magnetization distribution of a pinned domain wall.
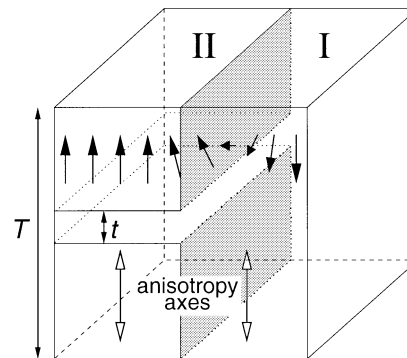

Fig. 4. Model geometry for domain wall pinning on a precipitation structure with parallel anisotropy axes. The shaded areas indicate the faces of the cells, where the magnetic domain wall gets pinned. The chain of arrows indicates the magnetization distribution of a pinned domain wall, which approaches the shaded faces of the cells.

crease toward the anisotropy field. Thus, in order to reach high pinning fields, a low ε_A ratio has to be achieved.

When the external field is switched on, the domain wall moves toward the interface and gets pinned. As the external field increases the Bloch wall is forced into the "harder material" until it depins and propagates further through the "harder material." The analytical result has been calculated with the one dimensional model of Kronmüller and Goll [6], which gives the pinning field as

$$H_{pin} = \frac{2K_1^{II}}{J_s^{II}} \frac{1 - \varepsilon_A \varepsilon_K}{\left(1 + \sqrt{\varepsilon_A \varepsilon_J}\right)^2}$$

where

$$\varepsilon_J = \frac{J_s^I}{J_s^{II}}, \qquad \varepsilon_A = \frac{A^I}{A^{II}}, \qquad \varepsilon_K = \frac{K_1^I}{K_1^{II}}$$

and I denotes the material parameters of the softer material and II those of the harder material.

IV. PINNING ON AN INTERCELLULAR PHASE (COHERENT PRECIPITATION)

The influence of the thickness t of an intercellular phase on coercivity has been investigated using a finite-element micromagnetic model with static energy minimization. As compared with the simple planar interface, we now have three regions (cf. Fig. 2). The outer regions (indicated with "I") represent the cells, whereas the center region (indicated with "II") represents the intercellular phase. In Sm(Co,Fe,Cu,Zr)$_z$ precipitation hardened magnets, the SmCo 2 : 17 cells are separated by a thin SmCo 1 : 5 intercellular phase. Depending on the Cu content of this cell boundary phase, its domain wall energy might be lower (high Cu

content) or higher (low Cu content) than that of the cells giving rise to "attractive" or "repulsive pinning," respectively.

In the former case, the domain wall prefers to stay in the intercellular phase, where it has a lower energy. However, its thickness has to be large enough so that the wall "fits in" [10]. Fig. 3 shows the dependence of the pinning field on the thickness of the intercellular phase in comparison with the ideal case of an intercellular phase of infinite thickness (where it reduces to "pinning on a planar interface"). Analogously, the intercellular phase has to be thick enough to provide an energy barrier in the case of repulsive pinning. The results are also shown in Fig. 3, where the axes have been scaled to the exchange length of the intercellular phase and the field to the pinning field for infinite thickness of the precipitation (which is 2200 kA/m in Sm(Co,Fe,Cu,Zr)$_z$ [6]). As a result, the thickness of the intercellular phase has to be at least three times the exchange length. This corresponds to the domain wall width (which is usually defined as $\pi \cdot l_{ex}$). For thinner precipitations the domain wall can either "tunnel" through the intercellular phase (repulsive pinning) or it does not fit into it (attractive pinning). Fig. 3 clearly emphasizes the similarity in behavior between attractive and repulsive pinning, which has not been covered in [10].

V. PINNING ON THE CELL STRUCTURE

Then the influence of the cell boundary phase perpendicular to the domain wall has been studied. The geometry is shown in Fig. 4. It resembles the situation of a domain wall, which moves from right to left and gets trapped in the (softer) intercellular
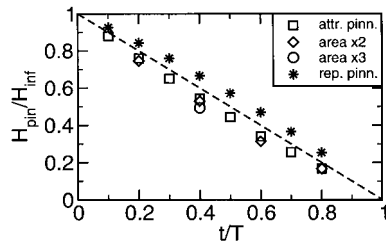
Fig. 5. Pinning field for repulsive pinning of a magnetic domain wall on the cell structure as a function of the relative thickness t/T. The data marked "area x2" and "area x3" have been obtained with a model scaled to twice and three times the initial size. The dashed line is just a guide to the eye.

phase ("I"), where it is repelled by the cells ("II"). The domain wall is pinned on the interface (indicated by the shaded areas in Fig. 4), but it tries to slip through the intercellular phase of thickness t, which separates the cells. The interesting question is, if the pinning field is changed by the cellular structure as compared with the perfect planar interfaces discussed here.

The results are given in Fig. 5, where the pinning field (normalized to the pinning field for $t = 0$, which corresponds to the planar interface again) is given as a function of the relative thickness t/T of the intercellular phase. T is the sum of the edge length of a cell and the thickness of the intercellular phase t. In Fig. 4 the "hard surface area" of the cells is indicated by the shaded faces. Obviously, the pinning field depends linearly on the relative thickness of the intercellular phase. Even if the cell size T and the thickness of the intercellular phase t are increased by a factor of two or three (cf. data marked "area x2" and "area x3" in Fig. 5) we find the same behavior, that the pinning field depends only on the ratio t/T.

If we switch to the case of repulsive pinning again, we can assume that now the cells ("II") are softer than the intercellular phase ("I") in Fig. 4. This time the domain wall moves from left to right and gets pinned in front of the intercellular phase. The pinning fields are also given in Fig. 5. They show the same linear behavior as in the case of attractive pinning.

For $Sm(Co,Fe,Cu,Zr)_z$ precipitation hardened magnets, this means, that the pinning field increases with the cell size. However, it decreases linearly with the thickness of the intercellular phase, if it is larger than the domain wall width. Below this limit

the pinning field is strongly reduced. These results are independent, whether attractive or repulsive pinning is dominating. Thus, the best magnetic properties should be found in magnets with large cells, thin (but still sufficiently thick) intercellular phases, and large differences in the domain wall energy (ideally, a large difference in the exchange constants).

VI. Conclusion

Our detailed study of the pinning behavior of domain walls has revealed, that the dependence of the pinning field on the thickness of the intercellular phase is equivalent for attractive and repulsive domain wall pinning. The cellular structure of $Sm(Co,Fe,Cu,Zr)_z$ magnets reduces the pinning field linearly with increasing relative thickness of the intercellular phase.

References

[1] G. C. Hadjipanayis, W. Tang, Y. Zhang, S. T. Chui, J. F. Liu, C. Chen, and H. Kronmüller, "High temperature 2 : 17 magnets: Relationship of magnetic properties to microstructure and processing," *IEEE Trans. Magn.*, vol. 36, pp. 3382–3387, Sept. 2000.

[2] J. Fidler and P. Skalicky, "Microstructure of precipitation hardened cobalt rare earth permanent magnets," *J. Magn. Magn. Mater.*, vol. 27, pp. 127–134, 1982.

[3] R. K. Mishra, G. Thomas, T. Yoneyama, A. Fukuno, and T. Ojima, "Microstructure and properties of step aged rare earth alloy magnets," *J. Appl. Phys.*, vol. 52, pp. 2517–2519, 1981.

[4] D. Süss, T. Schrefl, and J. Fidler, "Micromagnetic simulation of high energy density permanent magnets," *IEEE Trans. Magn.*, vol. 36, pp. 3282–3284, Sept. 2000.

[5] D. R. Fredkin and T. R. Koehler, "Hybrid method for computing demagnetizing fields," *IEEE Trans. Magn.*, vol. 26, pp. 415–417, Mar. 1990.

[6] H. Kronmüller and D. Goll, "Micromagnetic theory of the pinning of domain walls at phase boundaries," *Physica B: Condensed Matter*, vol. 319, pp. 122–126, 2002.

[7] K.-D. Durst, H. Kronmüller, and W. Ervens, "Investigations of the magnetic properties and demagnetization processes of an extremely high coercive $Sm(Co,Cu,Fe,Zr)_{7.6}$ permanent magnet I. Determination of intrinsic magnetic material parameters," *Phys. Statist. Sol. (a)*, vol. 108, pp. 403–416, 1988.

[8] W. Tang, A. M. Gabay, Y. Zhang, G. C. Hadjipanayis, and H. Kronmüller, "Temperature dependence of coercivity and magnetization reversal mechanism in $Sm(Co_{bal}Fe_{0.1}Cu_yZr_{0.04})_{7.0}$ magnets," *IEEE Trans. Magn.*, vol. 37, pp. 2515–2517, July 2001.

[9] E. Lectard, C. H. Allibert, and R. Ballou, "Saturation magnetization and anisotropy fields in the $Sm(Co_{1-x}Cu_x)_5$," *J. Appl. Phys.*, vol. 75, no. 10, pp. 6277–6279, May 1994.

[10] A. Aharoni, "Domain wall pinning at planar defects," *J. Appl. Phys.*, vol. 58, no. 7, pp. 2677–2680, Oct. 1985.